文章编号：1001-9014(2022)01-0305-06

DOI:10.11972/j.issn.1001-9014.2022.01.026

W-band dual-sheet beam traveling-wave tube with a novel planar slow-wave structure

DONG Yang, GUO Jing-Yu, WANG He-Xin, WANG Zhan-Liang, LU Zhi-Gang, GONG Hua-Rong, DUAN Zhao-Yun, GONG Yu-Bin, WANG Shao-Meng*

(National Key Laboratory on Vacuum Electronics, School of Electronic Science and Engineering, University of Electronic Science and Technology of China, Chengdu 610054)

Abstract: A dual-beam rectangular ring-bar (DBRRB) slow wave structure (SWS), which is with a planar structure and is suitable for micro fabrication, is proposed for W-band traveling-wave tubes (TWT). Supported by a pair of T-shaped dielectric rods, the RRB SWS is fit for dual-sheet beam operation. The high frequency characteristics are analyzed by using computer simulations. Wide bandwidth input-output structures adopting tapered structure and step waveguide are designed. Hot-test performance of the RRB SWS is investigated by means of Particle-in-cell (PIC) simulations. A solenoid magnetic field of 0.6 T is adopted to focus the sheet beams with voltage and current of 11.2 kV and 0.12 A. The saturated output power of 56.7 W at 94 GHz is obtained at the output port, corresponding a gain of 27.4 dB. In addition, an attenuator is added to suppress oscillations and achieve stable operation.

Key words: traveling wave tube, dual-sheet beam, step waveguide, attenuator

W波段双带状电子注新型平面慢波结构行波管

董 洋, 郭靖宇, 王禾欣, 王战亮, 路志刚, 巩华荣, 段兆云, 宫玉彬, 王少萌*

(电子科技大学 电子科学与工程学院,微波电真空器件国家级重点实验室,四川 成都 610054)

摘要:提出了一种适用于W波段行波管(TWT)的双注矩形环杆(DBRRB)慢波结构(SWS),该结构具有平面特性,适合于微细加工。在一对T形介质杆的支撑下,RRB SWS适用于双带状电子注工作。利用计算机仿真分析了其高频特性。设计并采用了渐变结构和阶梯波导的宽带输入输出结构。采用粒子(PIC)模拟研究了RRB SWS的热仿真性能,并用0.6 T的螺线管磁场,对电压和电流分别为11.2 kV和0.12 A的双带状注进行聚焦。仿真结果表明,在94 GHz时的饱和输出功率为56.7 W,对应的增益为27.4 dB。此外,还添加了一个衰减器来抑制振荡并实现了稳定工作。

关 键 词:行波管;双带状注;阶梯波导;衰减器

中图分类号:TN124　　**文献标识码**:A

Introduction

As the development of radar detection technology, the requirement on target resolution ratio becomes higher and higher. Thus, millimeter wave radar system has attracted researcher's attentions. W-band (75~110 GHz) is characterized by a large bandwidth and high resolution, which can be effectively utilized with lower atmospheric absorption, and it has an important application prospect in radar and satellite space communication [1]. The high-power devices in W-band are mainly vacuumed electron devices, including TWT [2], backward-wave oscillator (BWO) [3], gyrotron [4], etc., among them TWT has been widely investigated for its wide bandwidth.

Received date: 2021-04-01, **revised date**: 2021-05-28　　**收稿日期**:2021-04-01,**修回日期**:2021-05-28

Foundation items: Supported by National Natural Science Foundation of China (61921002, 61988102 and 62071087).

Biography: DONG Yang (1997-), male, Hunan, currently pursuing the PhD, School of Electronic Science and Engineering, University of Electronic Science and Technology of China (UESTC), Chengdu, China. Research area involves planar slow wave structure and radial klystron.
E-mail: 201921020403@std.uestc.edu.cn.

* **Corresponding author**: E-mail: wangsm@uestc.edu.cn

A slow wave structure is the core parts of a TWT. At W-band, the folded waveguide [5] has been the most popular slow wave structure for the advantages as high power and excellent heat dissipation. The cylindrical electron beam has been commonly used in folded waveguides, but as the structure size decreases, the cylindrical electron beam will suffer a strong space charge effect when the current is relatively large. Therefore, sheet electron beam becomes more and more popular with its weak space charge effect by increasing the width or height of the sheet beam.

There are several SWSs have been proposed and applied for W-band sheet-beam TWTs, including sine waveguide SWS [6], double-staggered grating SWS [7-8] and meander-line SWS [9-11]. In addition, the RRB SWS developed from the conventional ring-bar SWS is also suitable for sheet-beam TWT.

For the RRB SWS, reference [12] found that its ratio of backward-wave interaction impedance and forward-wave interaction impedance of the RRB SWS is lower than that of the planar helix with straight-edge connections (PH-SEC) SWS, indicating that the RRB SWS could operate more stability. In the reference [13], the RRB SWS based on dielectric substrates was presented, and its dispersion characteristics and interaction impedance were analyzed by using quasi-TEM approximation approach. The results show that the dispersion of the RRB SWS became weaker and the bandwidth became wider after adding dielectric substrates, and it has the characteristic of high gain.

In this paper, the DBRRB SWS is proposed for a W-band dual-sheet beam TWT. The high frequency characteristics have been investigated by using simulation. A wide band input-output structure has been proposed for the DBRRB SWS, leading to a good transmission curve. The hot performance of the DBRRB SWS, cooperating with two sheet electron beams, are obtained by using particle in cell (PIC) simulation.

1 High-frequency characteristics of the DBRRB SWS

Fig. 1 shows the single-period structure model of the DBRRB SWS, which consists of two rectangular rings and metal rods. The SWS is supported by a pair of T-shaped dielectric rods at the narrow sides. As a result, there are space for two sheet electron beams, locating along the broad sides. Although the inner tunnel of the rectangular ring has a higher interaction impedance than the outer side, the size of the inner tunnel is much smaller, leading to a higher current density and higher capture rate for electrons.

For a TWT, the lower the normalized phase velocity of the SWS is, the lower the operation voltage will be. And the higher the interaction impedance is, the stronger the wave interaction will be. For the proposed SWS, H and W are the height and width of the rectangular ring, L is the length of the metal rod, ed is the vertical distance between the electron beam and the SWS. The single period length of the SWS is $2*(L+dt)$, when dt is determined, L has great influence on the high frequency characteristics of the SWS. The CST Eigen-mode solver and HFSS are used to analyze the high frequency characteristics of the SWS. Fig. 2 shows the effect of parameter L on interaction impedance and normalized phase velocity of the SWS by CST. When L decreases, the normalized phase velocity will decrease and the interaction impedance will increase, which means that reducing L can decrease the working voltage and increase the degree of beam-wave interaction. Besides, the phase velocity is not linearly proportional to the period length ($v_{p1}/P_1 \neq v_{p2}/P_2$, $v_p/P=2\pi f/\varphi$) in the RRB SWS, for the reason of the phase shift changes with the period length, as shown in Fig. 3. The phase shift at 94 GHz increases by an average of 15° for every 0.04 mm increase in the period length.

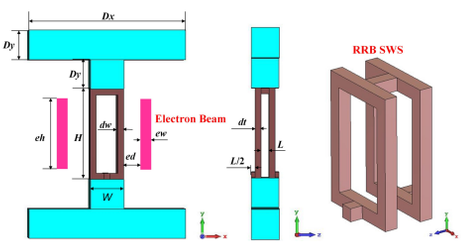

Fig. 1 The structure of the DBRRB SWS with T-shaped dielectric rods supporting
图1 T形介质杆支撑的DBRRB SWS结构模型

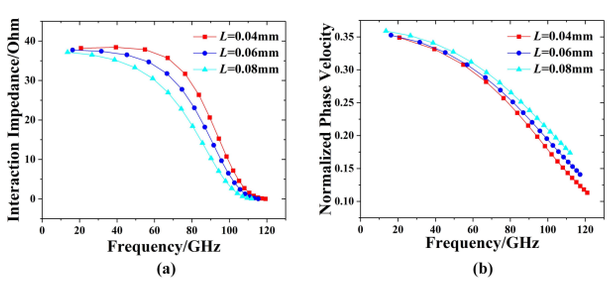

Fig. 2 The interaction impedance (a) and normalized phase velocity, (b) vary with L
图2 耦合阻抗(a)和归一化相速,(b)随L的变化

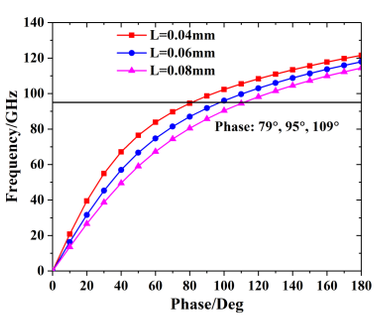

Fig. 3 The f-phase curve with different L
图3 不同L下的频率-相移图

W and H mainly affect the upper and lower cut-off frequencies of the fundamental mode of the slow-wave

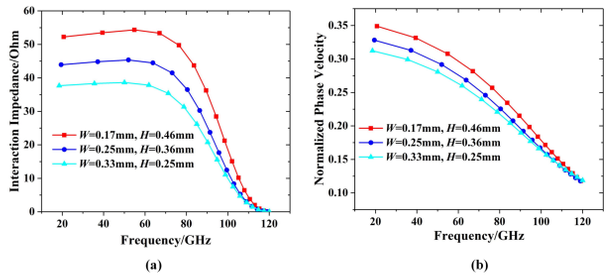

Fig. 4　The interaction impedance (a) and normalized phase velocity, (b) vary with *W/H*
图4　耦合阻抗(a)和归一化相速，(b)随W/H的变化

structure, and increasing *W* is beneficial to the focusing of the dual-sheet beam. When *W* increases, *H* needs to be reduced to keep the cut-off frequency of the fundamental mode consistent. Fig. 4 shows the variations of interaction impedance and normalized phase velocity with *W/H*, as can be seen, when *W/H* increases, the interaction impedance and normalized phase velocity will decrease.

Fig. 5 (a) shows the electric field distribution of the SWS along the direction of electron beam propagation in 94 GHz, which has axial field components, and the closer the electron beam to the SWS is, the stronger the electric field is and the higher the interaction impedance will be. From Fig. 5 (b), *ed* varies from 0.04 mm to 0.06 mm, the interaction impedance is about 28 Ω to 18 Ω in 94 GHz. When *ed* is set to 0.04 mm, the interaction impedance is about 36~15 Ω from 89~100 GHz in CST. And the interaction impedance curves calculated by CST and HFSS have the same trend with a little difference.

When the structural parameters of the SWS are determined, the dispersion curve of the SWS is confirmed

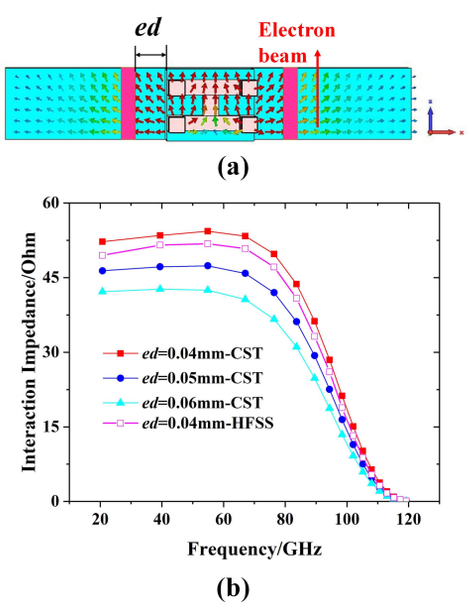

Fig. 5　(a) Axial electric field distribution of the SWS in 94GHz, (b) interaction impedance varies with *ed*
图5　(a)该慢波结构在94GHz处轴向电场分布，(b)耦合阻抗随ed的变化

and shown in Fig. 6. The dispersion curves calculated by CST and HFSS are consistent, which verifies the rationality of the design of the structure. The operation voltage at 94 GHz is calculated as 10.6 kV. The 10.6 kV beam line intersects with mode 1 and mode 2 at 94 GHz of working frequency point and 130 GHz of backward-wave frequency point, respectively. The interaction impedance of the backward-wave frequency point is about 10 Ω, which may cause oscillation in the TWT.

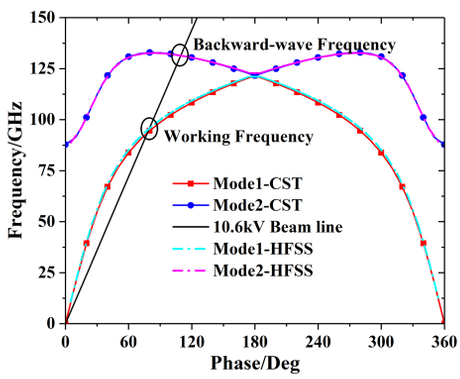

Fig. 6　The dispersion curves of the SWS
图6　慢波结构的色散曲线

2　Analysis of transmission characteristics

The simulation model of the whole TWT is shown in Fig. 7 (a), which includes the input and output coupling structure, the slow wave line (Molybdenum plated with Copper, conductivity of 2.8×10^7 S/m), dielectric rods (BN, relative dielectric constant of 3.8, loss tangent of 0.005), the attenuator and two cathodes. The attenuator, as shown in Fig. 7 (b), is designed to suppress backward-wave oscillation and reflection oscillation, the material is BeO with the relative dielectric constant of 6.5 and loss tangent of 0.5. The input-output coupling structure consists of two sections, one is the gradient structure, as shown in Fig. 7 (c), which includes three periods of gradient structure with a height ratio of *S*. The other section is a step waveguide, as shown in Fig. 7 (d), which transits the slow wave line to the WR-10 standard rectangular waveguide, and the size of WR-10 is 2.540 0 mm×1.270 0 mm.

The parameters of the TWT are listed in Table 1. The S-parameters of the step waveguide are investigated. The main parameters affecting the S-parameters of the step waveguide are *gx*1, *gx*2 and *gx*3, which can be optimized by adjusting the size and proportion between those parameters. From Fig. 8, we can see that the S11 of the step waveguide is lower than -15 dB in the whole W-band and the S21 is close to 0.

The attenuator divides the whole slow wave line into three segments with period numbers of *p*1=60, *p*2=10 and *p*3=80, respectively. The S-parameters of the whole simulation model are simulated by CST time domain solv-

Table 1 Parameters of the TWT (mm)
表1 行波管参数尺寸(mm)

Parameter	Value	Parameter	Value
L	0.04	*H*	0.46
W	0.17	*dt*	0.03
dw	0.03	*Dx*	0.80
Dy	0.15	*gx1*	0.81
gx2	0.38	*gx3*	0.08
gy	0.52	*L1*	0.07
L2	0.50	*L3*	1.00

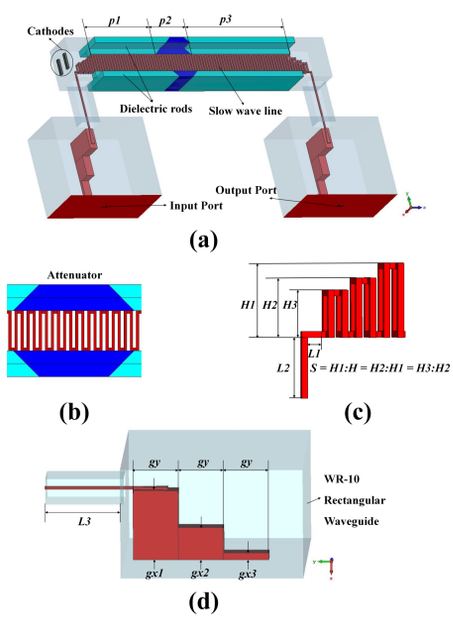

Fig. 7 (a) The whole TWT structure, (b) attenuator, (c) three periods gradient structure, (d) three-segment step waveguide
图7 (a)行波管整体结构,(b)衰减器,(c)三段周期渐变结构,(d)三段阶梯波导

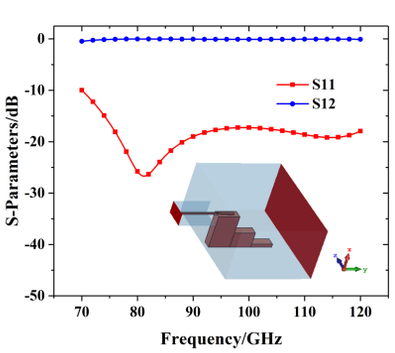

Fig. 8 S-parameters of the step waveguide
图8 阶梯波导的S参数

er, and the results are shown in Fig. 9. The parameter *S* is the height gradient ratio of the gradient structure and *S* =1 means there is no gradient structure. When *S*=0.8, the S11 parameter becomes better than *S*=1, which means the gradient structure can effectively improve the S11 of the TWT. As can be seen, the S11 is lower than -20 dB in the range of 83~113 GHz. From Fig. 8 (b), the S11 curves are almost the same with or without attenuator. The S21 without attenuator is -30 dB in 94 GHz duo to dielectric and metal loss, and after adding the attenuator the S21 is reduced to -60 dB.

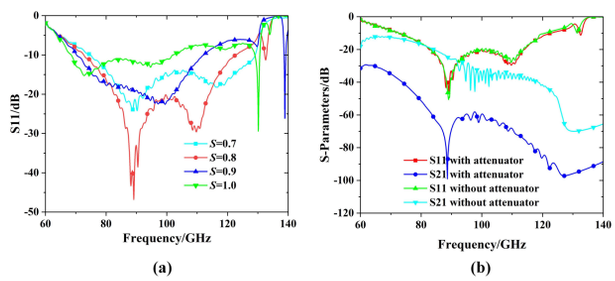

Fig. 9 (a) S11 with different *S* of the TWT, (b) S-parameters with or without attenuator
图9 (a)不同S下的S11,(b)加入衰减器后的S参数

3 Simulation of beam wave interaction

The beam wave interaction of the TWT is simulated by using CST particle-in-cell studio (CST-PIC). The PIC simulation of the TWT is carried out with the model in section-2, the attenuator has been added to suppress the possible oscillations, and good S-parameters have been obtained. Parameters that need to be optimized include the voltage and current of the electron beam, *p*3, *ed*, and the input power.

The height and width of the two identical cathodes are set as *eh*=0.4 mm and *ew*=0.08 mm respectively. And the vertical distance between the electron beam and the SWS is optimized to *ed*=0.04 mm, which is decided under the condition of electron interception loss and interaction impedance. The smaller the value of *ed* is, the stronger the interaction between the electron beam and the SWS is, and the higher the output power can be obtained. However, when it is too small, electrons will be captured by the SWS, resulting in electron interception loss. The optimized voltage and current of each electron beam are found as 11.2 kV and 0.06 A, respectively. The corresponding current density of each cathode is 187.5 A/cm^2, which can be further decreased by increasing the width or height of the cathode.

In addition, the focusing magnetic field is set to 0.6 T, and the number of periods of the SWS is 150. The output signals of the SWS after beam wave interaction is shown in Fig. 10 (a) as well as the input signal, from which the output power can be calculated as 56.7 W at 94 GHz with the input power of 0.1 W, corresponding a gain of 27.4 dB and electron efficiency of 4.2%. Besides, the output signals when there is no input signal have been investigated, as shown in Fig. 10 (b). It is clear that there are no oscillations for at least 20 ns simulation, indicating that no oscillation occurs without input power.

Fig. 11 shows the spectrum of the ports' signals, there is no indication of backward wave oscillation, as

the reflected signal is significantly lower than the incident signal and the frequency spectrum of output signal is relatively clean. That is to say, the attenuator has effectively suppressed the oscillations. Fig. 12 shows electron beam bunching and phase space diagram, as the interaction length increases, the number of electrons in the deceleration zone gradually exceeds that in the acceleration zone, and the energy of electrons is gradually exchanged to the high frequency field. Besides, the TWT is operating at a linear region and close to saturation in length.

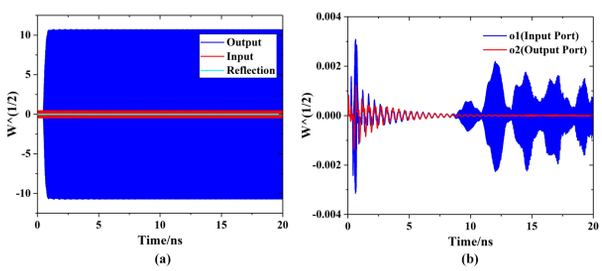

Fig. 10　The time-domain output signals with (a) and without, (b) input power
图10　有输入功率(a)和无输入功率,(b)的端口信号图

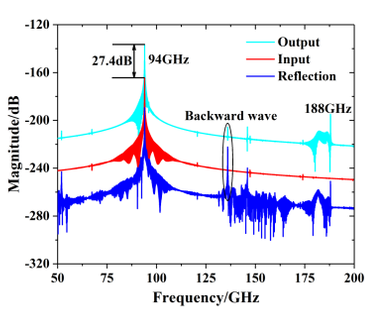

Fig. 11　The spectrum of signals
图11　信号频谱图

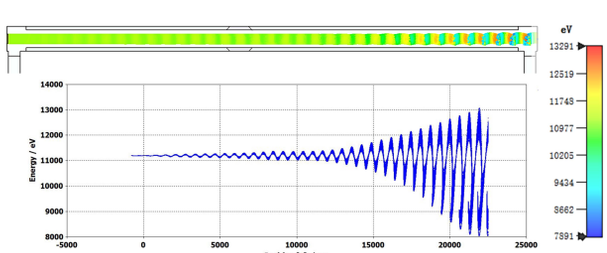

Fig. 12　Electron beam bunching and phase space diagram
图12　电子注群聚状态和相空间图

Fig. 13 shows the output power varies with beam width *ew* and beam height *eh*, while the beam current is retained. It can be seen that the increase of *eh* has little effect on output power. And the increase of *ew* has a greater impact on the output power, which is because of the interaction impedance decreases when goes far from the center of the slow wave structure. Fig. 14 shows the input-output power and gain curves, the saturated output power is 56.7 W when the input power of 0.1 W, and the gain decreases as the input power increases. The *f*-power and *f*-gain curves are shown in Fig. 15, the output power exceeds 20 W in the range of 91~96 GHz and the 3- dB bandwidth is close to 5 GHz.

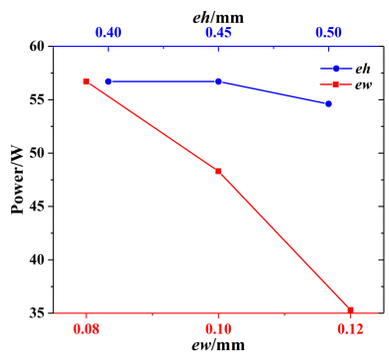

Fig. 13　The output power varies with *ew* and *eh*
图13　输出功率随电子注厚度 ew 和高度 eh 的变化

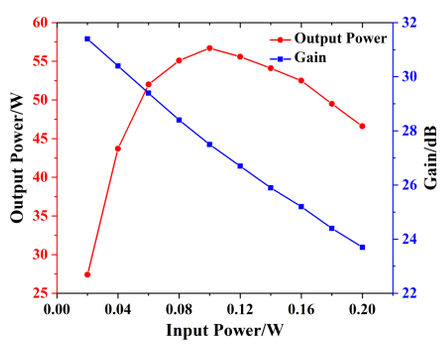

Fig. 14　The input-output power and gain curves
图14　输入-输出和增益曲线

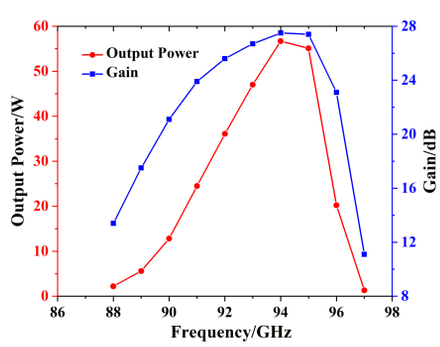

Fig. 15　The output power and gain vary frequency
图15　频率-输出和增益图

4　Conclusion

In this paper, the DBRRB SWS with T-shape dielectric rods supporting has been proposed for a W-band TWT. Good transmissions have been obtained with the addition of the gradient structure and the step wave-

guide. The oscillations were well suppressed by the addition of an attenuator. The beam wave interaction results show that the saturated output power is 56.7 W and the gain is 27.4 dB at 94 GHz under the condition of two sheet beams (11.2 kV, 0.12 A), 0.6 T focusing magnetic field and the input power of 0.1 W. The output power exceeds 20 W in the range of 91~96 GHz.

Acknowledgements

This work is supported by the National Natural Science Foundation of China (Grant Nos. 61921002, 61988102 and 62071087).

References

[1] Jebril A, Lucente M, Rossi T, *et al*. New developments in the WAVE W-band mission [C]. 2006 IEEE Aerospace Conference, 2006.

[2] Theiss A J, Meadows C J, Freeman R, *et al*. High-Average-Power W-band TWT Development [J]. *IEEE TRANSACTIONS ON PLASMA SCIENCE*, 2010, **38**(6): 1239-1243.

[3] Kumar M M A, Aditya S, WANG Shao-Meng. A W-band backward-wave oscillator based on planar helix slow wave structure [J]. *IEEE TRANSACTIONS ON ELECTRON DEVICES*, 2018, **65**(11): 5097-5102.

[4] Song H H, Mcdermott D B, Hirata Y, *et al*. Theory and experiment of a 94 GHz gyrotron traveling-wave amplifier [J]. *PHYSICS OF PLASMAS*, 2004, **11**(5): 2935-2941.

[5] FENG Jin-Jun, CAI Jun, HU Yin-Fu, *et al*. Development of w-band folded waveguide pulsed TWTs [J]. *IEEE TRANSACTIONS ON ELECTRON DEVICES*, 2014, **61**(6): 1721-1725.

[6] FANG S Z, XU J, LEI X, *et al*. Design of a W-band traveling-wave tube based on sine waveguide slow-wave structure with sheet electron beam [C]. 2019 International Vacuum Electronics Conference (IVEC), 2019.

[7] LU Zhi-Gang, WEN Rui-Dong, GE Wei-Hua, *et al*. Design of a low-gain high-power w-band sheet-beam traveling wave tube using a double-staggered grating slow wave structure [J]. *JOURNAL OF ELECTROMAGNETIC WAVES AND APPLICATION*, 2019, **33**(15): 1996-2008.

[8] LAI Jian-Qiang, GONG Yu-Bin, XU Xiong, *et al*. W-band 1-kw staggered double-vane traveling-wave tube [J]. *IEEE TRANSACTIONS ON ELECTRON DEVICES*, 2012, **59**(2): 496-503.

[9] Sengele S, Jiang Hong-rui, Booske J H, *et al*. Microfabrication and characterization of a selectively metallized w-band meander-line twt circuit [J]. *IEEE TRANSACTIONS ON ELECTRON DEVICES*, 2009, **56**(5): 730-737.

[10] SHEN Fei, WEI Yan-Yu, YIN Hai-Rong, *et al*. A novel v-shaped microstrip meander-line slow-wave structure for w-band mmpm [J]. *IEEE TRANSACTIONS ON PLASMA SCIENCE*, 2012, **40**(2): 463-469.

[11] SHEN Fei, WEI Yan-Yu, XU Xiong, *et al*. Symmetric double v-shaped microstrip meander-line slow-wave structure for w-band traveling-wave tube [J]. *IEEE TRANSACTIONS ON ELECTRON DEVICES*, 2012, **59**(5): 1551-1557.

[12] Chua C, Aditya S, Tsai J M, *et al*. Microfabricated Planar Helical Slow-Wave Structures Based on Straight-Edge Connections for THz Vacuum Electron Devices [J]. *Terahertz Science and Technology*, 2011, **4**(4): 208-229.

[13] FU Cheng-fang, ZHAO Bo, YANG Yu-dong, *et al*. Slow-Wave Characteristics of a Frame - Rod Structure Based on Micro-Fabricated Technology for THz Vacuum Electron Devices [J]. *Journal of Infrared Millimeter & Terahertz Waves*, 2016, **37**(11): 1106-1116.